A neutron diffraction study of macroscopically entangled proton states in the high temperature

phase of the KHCO$_3$ crystal at 340 K

A neutron diffraction study of macroscopically entangled proton states in the high temperature phase of the KHCO₃ crystal at 340 K

François Fillaux[1,4]**, Alain Cousson**[2] **and Matthias J Gutmann**[3]

[1] LADIR-CNRS, UMR 7075, Université P et M Curie, 2 rue Henry Dunant, 94320 Thiais, France
[2] Laboratoire Léon Brillouin (CEA-CNRS), CE Saclay, 91191 Gif-sur-Yvette, cedex, France
[3] ISIS Facility, Rutherford Appleton Laboratory, Chilton, Didcot OX11 0QX, UK

E-mail: fillaux@glvt-cnrs.fr

Abstract
We utilize single-crystal neutron diffraction to study the $C2/m$ structure of potassium hydrogen carbonate (KHCO₃) and macroscopic quantum entanglement above the phase transition at $T_c = 318$ K. Whereas split atom sites could be due to disorder, the diffraction pattern at 340 K evidences macroscopic proton states identical to those previously observed below T_c by Fillaux *et al* (2006 *J. Phys.: Condens. Matter* **18** 3229). We propose a theoretical framework for decoherence-free proton states and the calculated differential cross-section accords with observations. The structural transition occurs from one ordered $P2_1/a$ structure ($T < T_c$) to another ordered $C2/m$ structure. There is no breakdown of the quantum regime. It is suggested that the crystal is a macroscopic quantum object which can be represented by a state vector. Raman spectroscopy and quasi-elastic neutron scattering suggest that the $|C2/m\rangle$ state vector is a superposition of the state vectors for two $P2_1/a$-like structures symmetric with respect to (a, c) planes.

(Some figures in this article are in colour only in the electronic version)

1. Introduction

In principle, a crystal with perfect translational invariance is a macroscopic quantum systems with discrete phonon states at any temperature below melting or decomposition. However, for crystals containing O–H⋯O hydrogen bonds, there is a widely spread dichotomy of interpretation for the so-called 'proton disorder', usually observed as a dynamical equilibrium between two sites, say O1–H⋯O2 and O1⋯H–O2. For such systems, semiclassical approaches are commonly used to rationalize proton correlation times measured with solid-state NMR and quasi-elastic neutron scattering (QENS) [1]. Semiclassical protons are dimensionless particles, with definite positions and momentums, moving in a double well coupled to an incoherent thermal bath. Dynamics are rationalized with uncorrelated jumps over the barrier and 'incoherent tunnelling' through the barrier. In fact, these models describe a liquid-like surroundings and strong interaction with the thermal bath is supposed to lead to fast decoherence. By contrast, diffraction and vibrational spectra provide unquestionable evidences that the translational invariance and the quantum nature of lattice dynamics are not destroyed by proton transfer.

The crystal of potassium hydrogen carbonate, KHCO₃, is at variance with this dichotomy of interpretation [2–5]. This crystal is composed of centrosymmetric hydrogen bonded dimers (HCO₃⁻)₂, separated by potassium ions. Below ≈150 K, protons occupy sites corresponding to a unique configuration for dimers, say L. Between 150 and 300 K, protons are progressively transferred to the other

[4] Author to whom any correspondence should be addressed.
http://www.ladir.cnrs.fr/pagefillaux_eng.htm.

centrosymmetric configuration R, up to a population ratio R:$L \approx 18$:82. In contrast to semiclassical models, it has been observed that the sublattice of protons is a macroscopically entangled quantum object over the whole temperature range. Quantum correlations outside any description offered by classical physics are evidenced with neutrons because the intensity diffracted by the sublattice is proportional to the total nuclear cross-section $\sigma_H \approx 82.02$ b, instead of $\sigma_{Hc} \approx 1.76$ b for uncorrelated protons. Enhanced diffraction observed from cryogenic to room temperatures is consistent with a superposition of decoherence-free macroscopic states at thermal equilibrium and the correlation time measured with QENS [6] can be rationalized with quantum interferences [5]. There are therefore consistent evidences that protons in the crystal field are not semiclassical particles possessing properties on their own right [7].

In the present paper we examine whether the macroscopic entanglement is destroyed by the reversible structural phase transition at $T_c = 318$ K [8]. The population ratio R:L increases discontinuously to 0.5:0.5 and then remains a constant above T_c. This transition, supposed to be of the order–disorder type [9–17], could be of great significance to experimental studies of the quantum-to-classical interface in the crystalline state. However, structural and dynamical models are still in debate and require further studies. We have therefore conducted extensive single-crystal neutron diffraction measurements in order to (i) determine the best structural model; (ii) observe whether enhanced features due to quantum correlations survive or not above T_c. The experiments presented below show that the structural transition does not destroy the macroscopic quantum behaviour of protons. It transpires that the transition occurs from one ordered structure to another ordered structure through a coherent quantum process preserving the translational invariance of the crystal.

The organization of this paper is as follows. In section 2, we determine the structure at 340 K, for the sake of comparison with previous models. In section 3, we examine the total differential cross-section measured over a large **Q**-range, at the same temperature, which evidence the enhanced features of quantum correlations. The theoretical framework is presented in section 4 and we calculate the differential cross-section of correlated protons in section 5 for comparison with observations. In section 6, macroscopic states are opposed to statistical disorder and we utilize Raman spectroscopy to probe proton dynamics. We suggest that the crystal is in a pure state that can be represented by state vectors.

2. Crystal structure

The reversible structural transition has a very small enthalpy and the crystal retains its optical transparency [8]. Below T_c, the crystal symmetry is $P2_1/a$ with four indistinguishable KHCO$_3$ entities in the unit cell [3, 4, 18, 19]. Planar centrosymmetric dimers (HCO$_3^-$)$_2$, with O$\cdots$O distances of ≈ 2.58 Å, are practically parallel to (103) planes. They are alternately slightly tilted with respect to (a, c) glide planes.

Kashida and Yamamoto (KY) [9] have measured x-ray diffraction across the transition. The unit cell parameters are

Table 1. Neutron single-crystal diffraction data and structure refinement for potassium hydrogen carbonate at various temperatures. $\lambda = 0.8305$ Å, space group $P2_1/a$ at 300 K (after [4]) and $C2/m$ at 340 K (this work). The dimer symmetry is either C$_i$ or C$_{2h}$ in the two different structure models under consideration. The variance for the last digit is given in parentheses.

Crystal data	300 K	340 K C$_i$	340 K C$_{2h}$
a (Å)	15.18(1)	15.173(9)	15.173(9)
b (Å)	5.620(4)	5.628(4)	5.628(4)
c (Å)	3.710(4)	3.711(4)	3.711(4)
β (deg)	104.67(5)	104.63(5)	104.63(5)
Volume	306.2	306.6	306.6
Reflections measured	1731	1789	1789
Independent reflections	1475	931	931
Reflections used	1068	752	755
$\sigma(I)$ limit	3.00	3.00	3.00
Refinement on F			
R-factor	0.035	0.028	0.038
Weighted R-factor	0.034	0.019	0.037
Number of parameters	56	59	34
Goodness of fit	1.025	1.116	1.107
Extinction	3260(100)	15.4(4)	14.9(7)

very little affected, the symmetry above T_c is $C2/m$ and (a, c) glide planes become mirror planes. These authors envisaged two structural models: (i) the 'displacive' model based on reorientation of dimers whose symmetry changes from C$_i$ ($T \leqslant T_c$) to C$_{2h}$ above T_c; (ii) the 'disorder' model composed of split C$_i$ dimers, symmetric with respect to the mirror plane. This latter model was preferred by KY, but Machida *et al* [11] preferred C$_{2h}$ dimers to fit their neutron diffraction data.

We have collected single-crystal neutron diffraction data with the four-circle diffractometer 5C2 at the Orphée reactor (Laboratoire Léon Brillouin) [20]. The twinning-free crystal ($\approx 3 \times 3 \times 3$ mm^3), previously studied in [4] was loaded into an aluminium container heated at (340 ± 1) K. This temperature is sufficiently below decomposition (≈ 400 K) to avoid damage, and it is sufficiently high to marginalize critical phenomena [6, 8, 12–14]. The data reduction was carried out with CRYSTALS [21, 22].

We confirm the monoclinic C2/m (C$_{2h}^3$) symmetry and previous unit cell parameters (table 1) [9, 11]. Both structural models, referred to as 'C$_{2h}$' and 'C$_i$' in table 1, were refined. C$_{2h}$ dimers are composed of four O$_{1/2}$C$_{1/2}$OH$_{1/2}$ entities per unit cell, while C$_i$ dimers are obtained with four (HCO$_3$)$_{1/2}$ units. This latter model was refined in two steps. First, the split geometry was constrained to fit the mirror plane symmetry. Then, constraints were removed in order to check the stability. After further refinement, deviations were insignificant. The final R-factor is significantly better for the—therefore preferred—C$_i$ model (figure 1 and table 1), in accordance with KY, but at variance with Machida *et al*. The R-factor is slightly improved by further splitting protons in two sub-sites on either sides of dimer planes, separated by ≈ 0.05 Å. However, the large overlap of the thermal ellipsoids casts doubt on this splitting, so it is ignored in the remainder of this paper.

Table 2. Atomic positions, isotropic temperature factors and site occupancies for $KHCO_3$ at 340 K. The variance for the last digit is given in parentheses.

Atom	x/a	y/b	z/c	U (iso.) (Å^2)	Occupation
K(1)	0.165 26(7)	0.00	0.2957(3)	0.0290	1.00
C(1)	0.119 51(3)	0.5192(1)	−0.1437(1)	0.0186	0.50
O(1)	0.193 39(4)	0.5019(1)	0.0950(2)	0.0354	0.50
O(2)	0.078 1(2)	0.3021(1)	−0.264(1)	0.0337	0.50
O(3)	0.081 5(2)	0.6989(2)	−0.280(1)	0.0301	0.50
H(10)	0.017 6(2)	0.687(2)	−0.439(1)	0.0462	0.25
H(11)	0.018 9(2)	0.684(1)	−0.450(1)	0.0312	0.25

Table 3. Thermal parameters in Å^2 units for $KHCO_3$ at 340 K. The variance for the last digit is given in parentheses. The thermal parameters account for the variation of the contribution of each atom to Bragg's peak intensities through the thermal factor T^{at} depending on the reciprocal lattice parameters a^*, b^*, c^*, and unit cell indexes in reciprocal space h, k, l, as
$T^{at} = \exp[-2\pi^2(U_{11}^{at}h^2a^{*2} + U_{22}^{at}k^2b^{*2} + U_{33}^{at}l^2c^{*2} + 2U_{12}^{at}ha^*kb^* + 2U_{23}^{at}kb^*lc^* + U_{31}^{at}lc^*ha^*)]$.

| Atom	U_{11}	U_{22}	U_{33}	U_{23}	U_{13}	U_{12}
K(1)	0.0316(4)	0.0303(4)	0.0227(3)	0.000	0.0025(3)	−0.0003(1)
C(1)	0.0209(2)	0.0117(3)	0.0216(2)	0.0003(2)	0.0023(1)	−0.0001(2)
O(1)	0.0247(2)	0.0441(3)	0.0315(3)	−0.006(3)	−0.0036(2)	0.0083(1)
O(2)	0.029(1)	0.023(1)	0.041(2)	−0.0001(8)	−0.0067(9)	−0.0043(7)
O(3)	0.030(1)	0.028(1)	0.0295(9)	0.0018(7)	0.0009(7)	−0.0072(8)
H(10)	0.040(6)	0.034(5)	0.055(6)	−0.003(5)	−0.007(4)	0.003(4)
H(11)	0.034(5)	0.023(4)	0.036(5)	0.004(3)	−0.008(5)	−0.001(3)

Positional and thermal parameters for heavy atoms in tables 2 and 3 are quite consistent, within estimated errors, with those of KY, but more accurate. By contrast, the proton positions of KY, $x/a = 0.0323(32)$ and $z/c = -0.4102(123)$, are at variance with those in table 2 and the x-ray based O–H bond length of 0.762(52) Å is too short. These discrepancies could arise from the difference between the electronic and nucleus density. On the other hand, O–H bond lengths in table 4 are virtually identical to those of Machida *et al* for the C_{2h} model, and we have checked that the C_{2h} and C_i models refined with our data lead to identical proton positions. Furthermore, proton positions are identical to those previously reported at 14 and 300 K [3, 4], although with different occupancies.

The phase transition can be featured as follows: (i) the discontinuous change of the occupancy of proton sites, with no significant change in positions; (ii) small changes of K and O atom positions by ≈ 0.1 Å parallel to (*b*); (iii) the splitting of carbonate groups. The split carbon atoms separated by ≈ 0.2 Å along (*b*) can be distinguished, while the split oxygen atoms are practically indiscernible. The CO single and double bond lengths (1.395 and 1.210 Å, respectively in table 4) are markedly different from one another and from those at 300 K (1.333 and 1.273 Å, respectively [4]).

3. Total neutron scattering: measurements

In order to observe whether the enhanced features previously attributed to macroscopic entanglement survive above T_c, we have conducted diffraction experiments with the SXD instrument at the ISIS pulsed neutron source [23, 24]. The twinning-free crystal previously measured at 300 K ($\approx 15 \times 10 \times 3$ mm^3) was loaded in a vacuum tank at (340 ± 1) K. It was shown that multiple scattering effects are negligible [4].
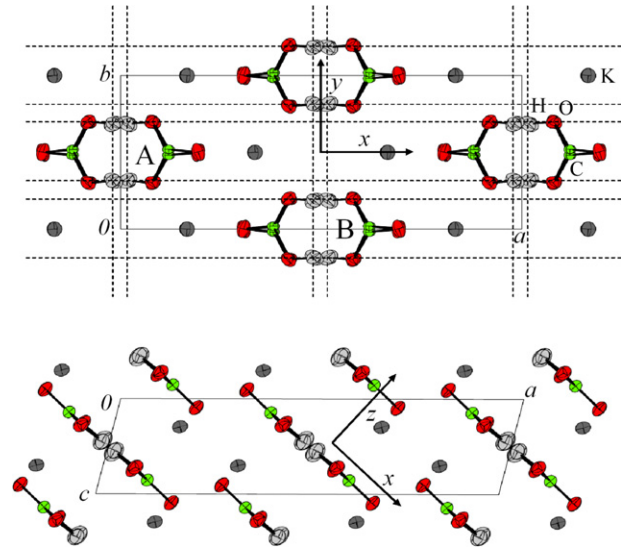
Figure 1. Schematic view of the crystalline structure of $KHCO_3$ at 340 K. The thin solid lines represent the unit cell. Top: projection onto the plane normal to *c*. The dotted lines joining protons emphasize the proton sublattice (see text). Bottom: projection onto (*a*, *c*).

Compared to the four-circle diffractometer, the advantage of SXD is twofold. Firstly, with the high flux of epithermal neutrons at the spallation source, one can measure a more extended domain of reciprocal space than at a reactor source. Secondly, with the time-of-flight technique, the total scattering function is measured at once and signals in addition to Bragg peaks are effectively collected.

By definition, Q_x, Q_y, Q_z, are projections of **Q** onto the normal mode axes for protons, x, y, z (figure 1). The maps
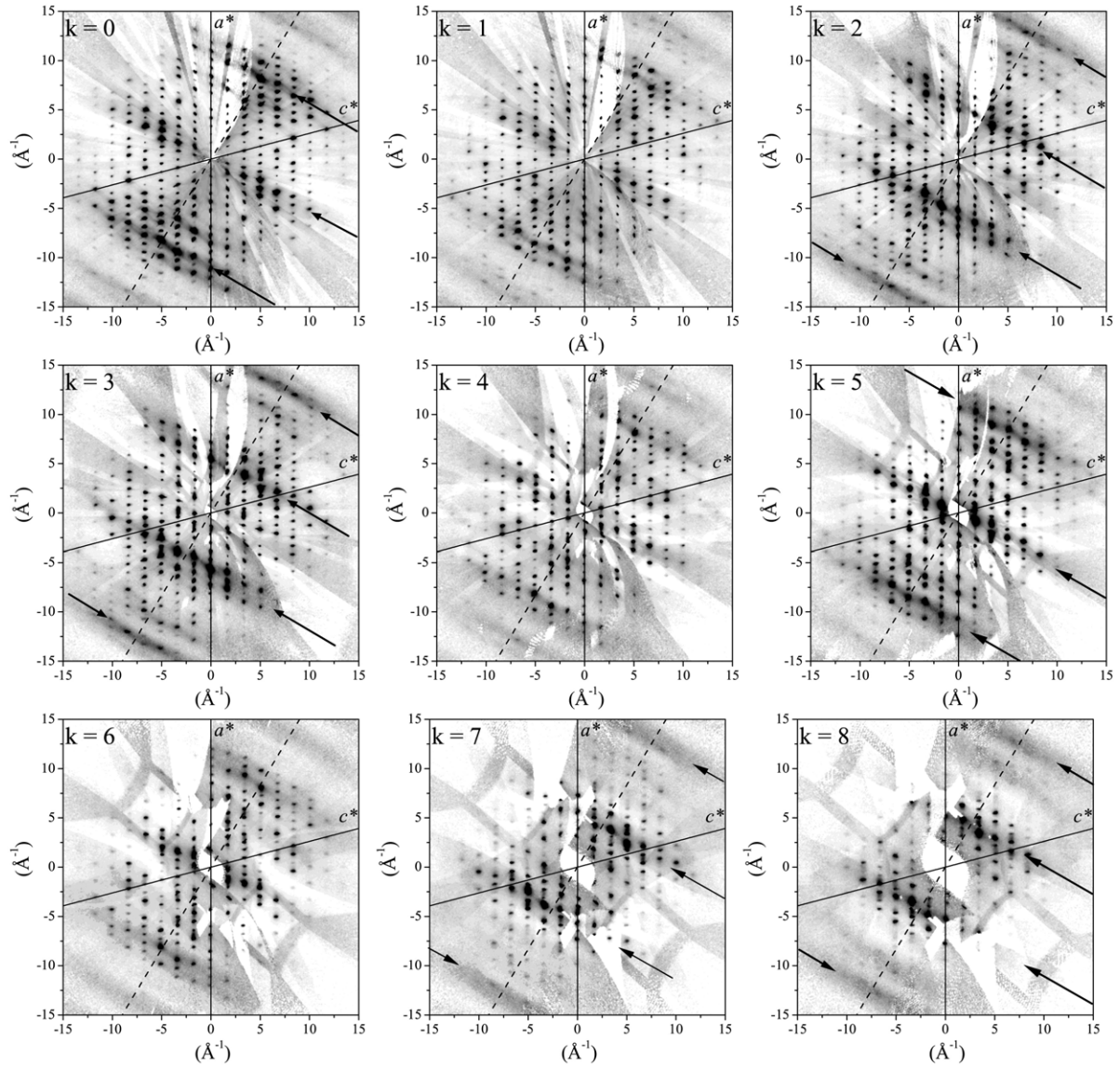
Figure 2. Diffraction patterns of $KHCO_3$ at 340 K in (a^*, c^*) planes. The arrows point to the ridges of intensity for momentum transfer parallel to (z) and perpendicular to the trace of dimer planes (dashed lines), which contain the (x) direction, as defined in figure 1. The (y) direction parallel to (b^*) is perpendicular to (a^*, c^*). $k = Q_y/b^*$ (see table 5).

of intensity (figures 2 and 3) for (a^*, c^*) planes at different k-values ($k = Q_y/b^*$, with $b^* \approx 1.112$ Å^{-1}) are concatenations of measurements for eight different crystal orientations, with $(b) \parallel (b^*)$ either parallel or perpendicular to the equatorial plane of the detector bank.

The anisotropic incoherent scattering intensity centred at $\mathbf{Q} = 0$, that was clearly observed at 15 K [3], is barely visible at 340 K. The shortfall of intensity with $|\mathbf{Q}|$ is a consequence, via the Debye–Waller factor, of the thermal population of the density of states [4, 25].

Cigar-like shaped ridges of intensity along Q_z are visible in figure 2 for particular k-values. For $k = 0$, they appear at $Q_x = 0$ and $\pm(10.00 \pm 0.25)$ Å^{-1}. For $k = 1$, they are barely visible. For $k = 2$ or 3, we observe a different pattern of ridges at $Q_x = \pm(5 \pm 0.2)$ and $\pm(15 \pm 0.2)$ Å^{-1}, still along Q_z. These features are best visible in figure 3 for $k = 2.5$. There is

no visible ridge at $k = 4$. Then, from $k = 5$ to 9, we observe the same sequence as for $k = 0$ to 4. These ridges are basically identical to those previously reported at 300 K or below for the ordered $P2_1/a$ crystal [3, 4]. Consequently, they are not due to transition induced phenomena, such as disorder, or domains, or planar faults, or critical behaviour [26]. Below it is shown that these features can be attributed to diffraction by the sublattice of entangled protons.

4. Theory

4.1. The adiabatic separation

Within the framework of the Born–Oppenheimer approximation, the vibrational Hamiltonian can be partitioned as

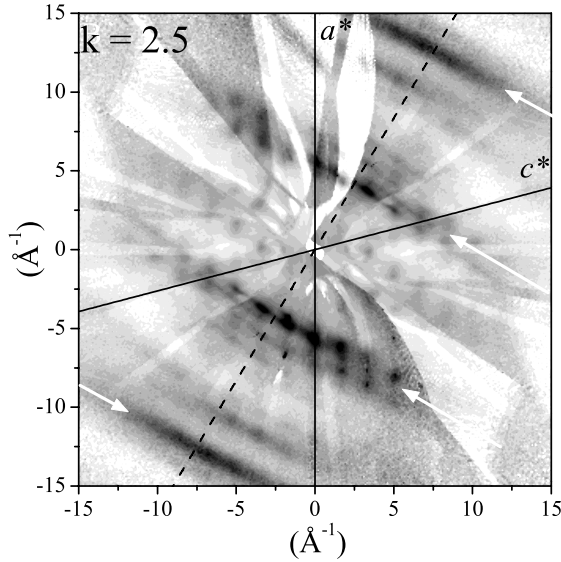$$\mathcal{H}_v = \mathcal{H}_H + \mathcal{H}_{at} + \mathcal{C}_{Hat}, \tag{1}$$

4

Figure 3. Map of scattering intensity for KHCO$_3$ at 340 K in between (a^*, c^*) reciprocal planes. The arrows emphasize ridges of intensity parallel to (z) and perpendicular to dimer planes.

Table 4. Interatomic distances in Å units in KHCO$_3$ at 340 K. The variance for the last digit is given in parentheses.

C(1)–O(1)	$\begin{cases} 1.245(1) \\ 1.247(1) \end{cases}$	O(3)–H(10)	1.002(1)
C(1)–O(2)	$\begin{cases} 1.395(1) \\ 1.210(1) \end{cases}$	O(3)–H(11)	1.003(1)
C(1)–O(3)	$\begin{cases} 1.210(1) \\ 1.395(1) \end{cases}$	H(10)–H(11)	$\begin{cases} 0.053(3) \\ 0.601(1) \end{cases}$
C(1)–C(1)	0.216(1)	H(10)–H(10)	0.607(1)
O(1)–O(1)	0.02(1)	H(11)–H(11)	0.599(1)
O(2)–O(3)	0.09(1)		
O(2)–H(10)	0.983(1)	O(2)–H(11)	0.988(1)

where $\mathcal{H}_H$ and $\mathcal{H}_{at}$ represent the sublattices of protons (H$^+$) and heavy atoms, respectively, while $\mathcal{C}_{Hat}$ couples the subsystems. For OH$\cdots$O hydrogen bonds, coupling terms between OH and O$\cdots$O degrees of freedom are rather large [27, 28], and beyond the framework of the perturbation theory. Two approaches, either semiclassical or quantum, are commonly envisaged.

Semiclassical protons are dimensionless particles, with definite positions and momentums, moving across a potential hypersurface [29–33]. Complex trajectories involving heavy atoms lead to mass renormalization, and to incoherent phonon-assisted tunnelling [1, 6, 34]. This approach is quite natural when the Born–Oppenheimer surface is calculated from first principles, but quantum effects are severely underestimated.

Alternatively, if the classical concept of 'trajectory' is abandoned, adiabatic separation of $\mathcal{H}_H$ and $\mathcal{H}_{at}$ may lead to tractable models [4, 28, 31, 35–37]. Then, protons in a definite eigenstate should remain in the same state in the course of time, while heavy atoms oscillate slowly, in an adiabatic hyperpotential depending on the proton state, through the coupling term. This separation is relevant for KHCO$_3$ because adiabatic potentials for different protons states do not intersect each other. In fact, the separation is rigorously exact in the ground state, since protons should remain in this state for ever, if there is no external perturbation. Then, protons are bare fermions and quantum correlations arise [4].

4.2. Macroscopic proton states

Consider a crystal composed of very large numbers N_a, N_b, N_c ($\mathcal{N} = N_a N_b N_c$) of unit cells labelled j, k, l, along crystal axes (a), (b), (c), respectively. Because centrosymmetric dimers have no permanent electric dipole, interdimer coupling terms are negligible [38–40]. Proton dynamics for a C$_i$ dimer is modelled with collinear oscillators in three dimensions, along

coordinates α_{1jkl} and α_{2jkl} ($\alpha = x, y, z$) with respect to equilibrium positions at $\pm\alpha_{0jkl}$. The mass-conserving normal coordinates and their conjugated momentums,

$$\alpha_s = \frac{1}{\sqrt{2}}(\alpha_1 - \alpha_2 + 2\alpha_0), \qquad P_{s\alpha} = \frac{1}{\sqrt{2}}(P_{1\alpha} - P_{2\alpha}),$$

$$\alpha_a = \frac{1}{\sqrt{2}}(\alpha_1 + \alpha_2), \qquad P_{a\alpha} = \frac{1}{\sqrt{2}}(P_{1\alpha} + P_{2\alpha}),$$
(2)

lead to uncoupled oscillators at frequencies $\hbar\omega_{s\alpha}$ and $\hbar\omega_{a\alpha}$, respectively, each with $m = 1$ amu. The difference $\hbar\omega_{s\alpha} - \hbar\omega_{a\alpha}$ depends on the coupling term (say λ_α). The wavefunctions, namely $\Psi^a_{njkl}(\alpha_a)/\sqrt{2}$, $\Psi^s_{n'jkl}(\alpha_s - \sqrt{2}\alpha_0)/\sqrt{2}$ for a half-dimer, cannot be factored into wavefunctions for individual particles, so there is no local information available for these entangled oscillators and the degenerate ground state must be antisymmetrized. For this purpose, the wavefunctions are rewritten as linear combinations of those for permuted oscillators as

$$\frac{1}{\sqrt{2}}\Theta_{0jkl\pm} = \frac{1}{2}\prod_\alpha \Psi^a_{0jkl}(\alpha_a)[\Psi^s_{0jkl}(\alpha_s - \sqrt{2}\alpha_0)$$
$$\pm \Psi^s_{0jkl}(\alpha_s + \sqrt{2}\alpha_0)],$$
(3)

where $\Theta_{0jkl\pm}$ is the total wavefunction for superposed half-dimers with identical proton sites. Then, the antisymmetrized state vectors are:

$$|0jkl+\rangle \otimes |S\rangle = |\Theta_{0jkl+}\rangle \otimes \frac{1}{\sqrt{2}}[|\uparrow_1\downarrow_2\rangle - |\downarrow_1\uparrow_2\rangle];$$

$$|0jkl-\rangle \otimes |T\rangle = |\Theta_{0jkl-}\rangle \otimes \frac{1}{\sqrt{3}}\Big[|\uparrow_1\uparrow_2\rangle + |\downarrow_1\downarrow_2\rangle$$
(4)
$$+ \frac{1}{\sqrt{2}}[|\uparrow_1\downarrow_2\rangle + |\downarrow_1\uparrow_2\rangle]\Big].$$

The oscillators are now entangled in position, momentum, and spin. In contrast to magnetic systems [41], there is no level splitting, so the symmetry-related entanglement is energy free. It is also independent of the magnitude of the coupling terms between oscillators. Furthermore, in contrast to Keen and Lovesey [42], or Sugimoto *et al* [43], we argue, as an experimental fact, that there is no significant exchange integral for protons separated by ≈ 2.2 Å [44]. Protons in KHCO$_3$ are definitely not itinerant particles with an energy band structure.

The spatial periodicity of the crystal leads to extended states and nonlocal observables in three dimensions. Consider the vibrational wavefunction for a unit cell containing two dimer entities as $\Xi_{0jkl\tau} = \Theta_{0jkl\tau} \pm \Theta'_{0jkl\tau}$, with $\tau =$ '+' or '−'. Then, trial phonon waves can be written as

$$\Xi_{0\tau}(\mathbf{k}) = \frac{1}{\sqrt{\mathcal{N}}} \sum_{l=1}^{N_c} \sum_{k=1}^{N_b} \sum_{j=1}^{N_a} \Xi_{0jkl\tau} \exp(i\mathbf{k} \cdot \mathbf{L}), \qquad (5)$$

where $\mathbf{k}$ is the wavevector and $\mathbf{L} = j\mathbf{a} + k\mathbf{b} + l\mathbf{c}$, with the unit cell vectors $\mathbf{a}$, $\mathbf{b}$, $\mathbf{c}$. For fermions, antisymmetrization leads to

$$\mathbf{k} \cdot \mathbf{L} \equiv 0 \text{ modulo } 2\pi. \qquad (6)$$

Consequently, there is no phonon (no elastic distortion) in the ground state. This symmetry-related 'super-rigidity' [4] is independent of proton–proton interaction. Then, state vectors in three dimensions can be written as:

$$\begin{aligned} |\Xi_{0+}(\mathbf{k} = \mathbf{0})\rangle \otimes |S\rangle; \\ |\Xi_{0-}(\mathbf{k} = \mathbf{0})\rangle \otimes |T\rangle. \end{aligned} \qquad (7)$$

There is no local information available for these entangled states and the wavefunctions $\Xi_{0\tau}(\mathbf{k} = \mathbf{0})$ describes oscillations of the super-rigid sublattice as a whole. Finally, the ground state of the sublattice is:

$$\begin{aligned} \sqrt{\mathcal{N}}|\Xi_{0+}(\mathbf{k} = \mathbf{0})\rangle \otimes |S\rangle; \\ \sqrt{\mathcal{N}}|\Xi_{0-}(\mathbf{k} = \mathbf{0})\rangle \otimes |T\rangle. \end{aligned} \qquad (8)$$

This state is intrinsically steady against decoherence. Irradiation by plane waves (photons or neutrons) may single out some excited states. Entanglement in position and momentum is preserved, while the spin symmetry and super-rigidity are destroyed. However, these features are reset automatically after decay to the ground state, presumably on the timescale of proton dynamics. This mechanism allows the super-rigid sublattice to be at thermal equilibrium with the surroundings, despite the lack of internal dynamics. Note that even at room temperature, the thermal population of the first excited proton state ($\gamma \text{OH} \approx 1000 \text{ cm}^{-1}$) is negligible ($<1\%$).

5. Differential cross-section: calculations

Neutrons (spin $1/2$) are unique to observing the spin symmetry of proton states (7). However, the spin symmetry is not stabilized by any energy. It is therefore extremely fragile and only 'noninvasive' experiments, free of measurement induced decoherence, can evidence quantum entanglement [45]. For neutron scattering, this means (i) no energy transfer, (ii) no spin flip and (iii) particular $\mathbf{Q}$-values preserving the super-rigidity. For planar dimers, these conditions are realized when Q_x, Q_y, match a node of the reciprocal sublattice of protons, so that scattering events probe the super-rigid lattice without any perturbation of its internal state. The spin symmetry is probed along the neutron spin direction without spin flip and the cross-section, namely the total nuclear cross-section σ_H, is ≈ 45 times greater than the coherent cross-section,

σ_{Hc}, when the matching conditions are not realized [4, 46]. Enhanced diffraction probe the perfect periodicity of the super-rigid sublattice, so the Debye–Waller factor is equal to unity. Alternatively, when the matching conditions are not realized, phonons created by neutrons contribute to the thermal parameters in table 3 and to the ellipsoids in figures 1.

In fact, enhanced diffraction and Bragg peaks of heavy atoms are superimposed. Their intensities are proportional to σ_H and $\sigma_{cKCO_3} \exp\{-2W_{KCO_3}(\mathbf{Q})\}$, respectively, where $\sigma_{cKCO_3} \approx 27.7$ b is multiplied by the Debye–Waller factor. At large $\mathbf{Q}$-values, the contribution of heavy atoms is largely hidden by that of correlated protons, and this effect is more pronounced at elevated temperatures.

The dashed lines in figure 1 show that proton sites are aligned along x and y, but not along z. Consequently, the noninvasive condition can be realized for Q_x and Q_y exclusively, whereas Q_z never coincides with a node of the reciprocal lattice of protons. Then, the diffraction pattern depends on whether we consider incoherent or coherent scattering along Q_z.

In order to calculate the differential scattering functions, we consider a $C2/m$ super-rigid sublattice composed of primitive unit cells $(a/2, b, c)$ with (j, k, l) indexes. Proton sites are at $\pm\{x_{0jkl}, y_{0jkl}, 0\}$, $\pm\{x_{0jkl}, -y_{0jkl}, 0\}$, with respect to the centre of split dimers. The periodicity of the grating-like structure parallel to y is $D_x/2$, with $D_x \approx a/\cos 42° \approx 20.39$ Å, while the periodicity of double lines parallel to x is $D_y = b$.

5.1. Super-rigid arrays in two dimensions

The differential cross-section can be written as

$$\begin{aligned} \frac{d\sigma_2}{d\Omega} \propto \sum_{l=1}^{N_c} \sum_{\tau_i} \sum_{\tau_f} \Bigg| \sum_{j=1}^{N_a'} \sum_{k=1}^{N_b} &\{[\exp iQ_y(kD_y - y_0) \\ &+ \tau_i\tau_f \exp iQ_y(kD_y + y_0)][\exp iQ_x(jD_x/2 - x_0) \\ &+ \tau_i\tau_f \exp iQ_x(jD_x/2 + x_0)]\}^2 \Bigg|^2 \exp -2W_z(Q_z), \qquad (9) \end{aligned}$$

with $N_a' = 2N_a$. Neutrons are scattered either in-phase ($\tau_f\tau_i = +1$) or anti-phase ($\tau_f\tau_i = -1$) by pairs of lines separated by $2x_0 \approx 0.6$ Å and $2y_0 \approx 2.209$ Å, respectively. The phase matching condition, namely x_0 (y_0) commensurable with $D_x/2$ (D_y), is intrinsic to the crystal structure. $\{\cdots\}^2$ accounts for simultaneous scattering by superposed singlet-like and triplet-like states (7), without neutron spin flip. The compound Debye–Waller factor $\exp -2W_z(Q_z)$, including contributions from all atoms, accounts for incoherent scattering along Q_z.

The diffraction pattern is composed of rods of diffuse scattering parallel to Q_z, cigar-like shaped by the Debye–Waller factor, at Q_x, Q_y-values corresponding to divergences of (9) gathered in table 5. Such divergences occur at $Q_y = n_y\pi/y_0 \approx n_y \times 2.86$ Å^{-1}, since $Q_yD_y/\pi \approx 5n_y$ is integer. There is no divergence for anti-phase scattering at $Q_y = \pm(n_y + 1/2)\pi/y_0$, because $Q_yD_y/\pi \approx 5(n_y + 1/2)$ is not integer. For n_y even, Q_yD_y/π is also even, $\tau_i = \tau_f$, and ridges are anticipated at $Q_x = n_x\pi/x_0 \approx n_x \times 10$ Å^{-1},

Table 5. Orders n_y, n_x and positions Q_y, Q_x of rods of intensity arising from the entangled array of orthogonal double lines of protons in two dimensions. Obs. Q_x: positions in Å^{-1} of the observed rods of intensity along Q_z in figures 2 and 3. $Q_y D_y/\pi$ is rounded to integers.

n_y	$\tau_i \tau_f$	Q_y (Å^{-1})	$Q_y D_y/\pi$	$k = Q_y/b^*$	Q_x	Obs. Q_x (Å^{-1})
0	+1	0	0	0	$n_x \pi/x_0$	0, ±10
1	−1	2.86	5	2.57	$(n_x + 1/2)\pi/x_0$	±5, ±15
2	+1	5.71	10	5.14	$n_x \pi/x_0$	0, ±10
3	−1	8.57	15	7.71	$(n_x + 1/2)\pi/x_0$	±5, ±15

since $Q_x D_x/\pi \approx 68 n_x$ is even. Alternatively, for n_y odd, $Q_y D_y/\pi$ is also odd, $\tau_i \neq \tau_f$, and ridges are anticipated at $Q_x = (n_x + 1/2)\pi/x_0$, since $Q_x D_x/\pi \approx 68(n_x + 1/2)$ is even. In this case, the enhanced features are best visible at $k \approx 2.57$ (figure 3).

5.2. Super-rigid lattice in three dimensions

The differential cross-section for no spin flip scattering events is

$$
\begin{aligned}
\frac{d\sigma_3}{d\Omega} \propto \sum_{\tau_i} \sum_{\tau_f} \Bigg| \sum_{j=1}^{N'_a} \sum_{k=1}^{N_b} \sum_{l=1}^{N_c} \exp i Q_z l D_z \\
\times \{[\exp i Q_y(k D_y - y_0) + \tau_i \tau_f \exp i Q_y(k D_y + y_0)] \\
\times [\exp i Q_x (j D_x/2 - x_0) \\
+ \tau_i \tau_f \exp i Q_x(j D_x/2 + x_0)]\}^2 \Bigg|^2 .
\end{aligned}
\tag{10}
$$

Divergences occur along the previous rods of intensity at $Q_z = \pm n_z 2\pi/D_z$, with $D_z \approx c \times \cos 28° \approx 3.28$ Å and $2\pi/D_z \approx 1.92$ Å^{-1}. In figure 2, these peaks clearly emerge from the rods of diffuse scattering depressed by the Debye–Waller factor in (9).

Equations (9) and (10) confirm that the enhanced features correspond to the reciprocal sublattice of protons represented by state vectors (8) based on a theoretical framework free of ad hoc hypothesis or parameters. The only prerequisite, namely the adiabatic separation, is an intrinsic property of hydrogen bonds in this crystal. By contrast, other models [42, 43] cannot account for enhanced diffraction.

6. Discussion

Kashida and Yamamoto [9] have opposed the ordered C_{2h} to the disordered C_i structures. The argument consists in that for the former there is no splitting of heavy atom sites and the symmetrized double wells for protons lead to quantum delocalization [6, 14, 16, 17, 47]. By contrast, split C_i dimers are supposed to be representative of a statistical distribution of atom positions and the double well remains asymmetric, as it is below T_c.

Kashida and Yamamoto [9] or Eckold *et al* [6] have observed that the $P2_1/a$ superlattice reflections ($h + k = 2n+1$) merge above T_c into elastic diffuse scattering, cigar-like shaped along (a^*). The intensity decreases as the temperature increases but the signal is still visible above 340 K. According to KY, the $P2_1/a$ local structure could survive above T_c as pre-transitional domains whose correlation length diverges as T

goes down to T_c. Diffuse scattering along (a^*) is invisible with SXD (figure 2) but this does not question the existence of this signal.

Critical phenomena have been also thoroughly investigated for the phase transition of KDCO$_3$ at $T_{cD} = 353$ K, taking advantage of the larger coherent scattering cross-section of the deuterium atom [12–14]. QENS measurements at the superlattice reflection (1, 2, 0) with the high resolution spin-echo technique evidence very slow dynamics ($\sim 10^{-9}$ s) above T_{cD} and complete slowing down as $T \longrightarrow T_{cD}$. These dynamics were tentatively associated with pre-transitional collective re-orientation of dimers, eventually correlated with the softening of an acoustic mode propagating along (a^*), with polarization parallel to (b) [8]. On the other hand, diffuse scattering around the main reflection (0, 2, 0) was attributed to the relaxation of individual dimers [12–14].

In contrast to the order–disorder schemes envisaged in previous works, the diffraction patterns presented in figures 2 and 3 lead to the conclusion that the structural transition is of the order–order type. Then the question arises as to whether the double well undergoes symmetrization or not.

The shape of the double wells along the hydrogen bonds can be probed with Raman spectroscopy in the frequency range of the OH stretching vibrations [5, 48]. In figure 5, the submaxima observed below T_c at $\approx$2580, 2800, 2930, 3100 cm^{-1} are representative of the four transitions for the asymmetric double wells of the $P2_1/a$ structure. Additional transitions (for example overtones and combinations) cannot be excluded, but a detailed assignment scheme is not necessary because the chief point of the argument is that symmetrization of the double wells above T_c should be of dramatic consequences to the spectral profile: (i) large frequency shifts due to the collapse of the potential asymmetry; (ii) the symmetry-related selection rules should extinguish two among the four transitions. Figure 5 shows that the extended eigenstates of the νOH mode probed at the Brillouin zone centre are identical for the $P2_1/a$ and $C2/m$ structures. Symmetrization is excluded.

The $C2/m$ structure can be featured as follows. Firstly, enhanced diffraction suggests that the crystal is in a pure state ($|C2/m\rangle$) composed of extended states for all dynamical degrees of freedom. Secondly, Raman spectra suggest that $|C2/m\rangle$ can be represented with a superposition of state vectors $|P_u\rangle$ and $|P_d\rangle$ representing $P2_1/a$-like substructures, symmetric with respect to (a, c). They are labelled with 'up' (u) and 'down' (d) orientations of a pseudospin along z. According to the quantum theory of measurements [7, 49, 50], the eigenstates of either $|P_u\rangle$ or $|P_d\rangle$ are probed with Raman.
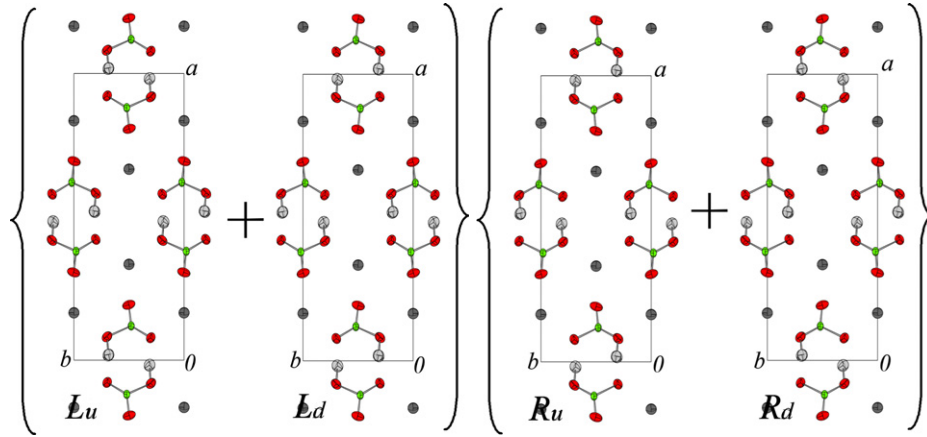
Figure 4. Schematic representation of the L_u, L_d, and R_u, R_d, $P2_1/a$-like configurations corresponding to state vectors superposed in the $|C2/m\rangle$ crystal state above T_c (see text). L and R correspond to different configurations for protons in dimers. Configurations u and d are symmetric with respect to (a, c). Each site is half-occupied.
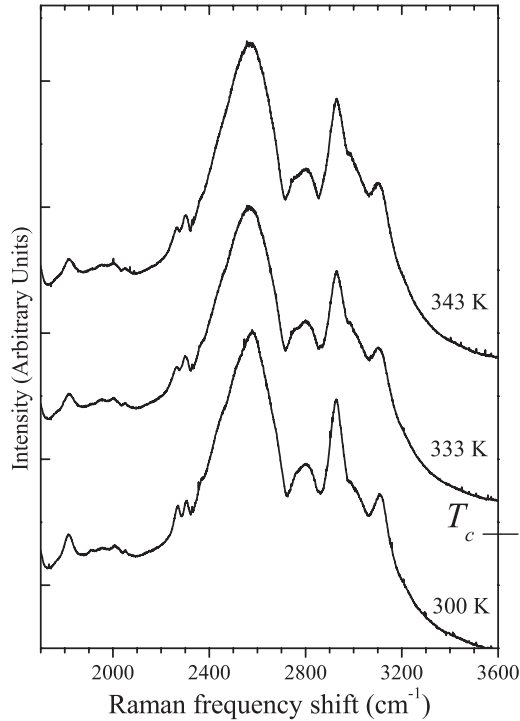

Figure 5. Raman spectra of powdered $KHCO_3$ crystal across the phase transition at $T_c = 318$ K. The spectra were recorded with a DILOR XY triple-monochromator equipped with an Ar^+ laser emitting at 4880 Å. The spectral resolution was ≈ 2 cm^{-1}. The sample was sealed in a glass tube and then loaded in a furnace. The temperature was controlled within ± 2 K.

For each substructure, there are two configurations, L or R, for the proton sublattice. Within the framework of the adiabatic separation, the state vectors of the four configurations L_u, R_u, L_d, R_d, sketched in figure 4, are $|p_u\rangle|H_{Lu\tau}\rangle|\tau\rangle$, $|p_u\rangle|H_{Ru\tau}\rangle|\tau\rangle$, $|p_d\rangle|H_{Ld\tau}\rangle|\tau\rangle$, $|p_d\rangle|H_{Rd\tau}\rangle|\tau\rangle$, where $|p_u\rangle$ and $|p_d\rangle$ represent heavy atoms. The ground state is a superposition of the degenerate states $|p_u\rangle|H_{Lu\tau}\rangle|\tau\rangle$ and $|p_d\rangle|H_{Ld\tau}\rangle|\tau\rangle$, while $|p_u\rangle|H_{Ru\tau}\rangle|\tau\rangle$ and $|p_d\rangle|H_{Rd\tau}\rangle|\tau\rangle$, also degenerate, are at higher energy (ΔE_{LR}). The state vector of the crystal can be

then written as

$$|C2/m\rangle = 2^{-1/2}\{\alpha(T)[|p_u\rangle|H_{Lu\tau}\rangle + |p_d\rangle|H_{Ld\tau}\rangle]$$
$$+ \beta(T)[|p_u\rangle|H_{Ru\tau}\rangle + |p_d\rangle|H_{Rd\tau}\rangle]\}|\tau\rangle, \qquad (11)$$

with $\alpha(T)^2 + \beta(T)^2 = 1$. The superposition of proton states is consistent with enhanced diffraction because the corresponding sublattices are identical in reciprocal space.

QENS measurements of $KHCO_3$ [6] are also consistent with (11). The inverse correlation time for proton transfer ($\tau_0^{-1} \approx 2 \times 10^{12}$ s^{-1}) is temperature independent, without any discontinuity at T_c, because QENS, like Raman spectroscopy, probes proton dynamics of the $P2_1/a$ structure below T_c and the same dynamics for either $|P_u\rangle$ or $|P_d\rangle$ above T_c.

Furthermore, τ_0^{-1} below T_c is consistent with a superposition of proton states giving rise to quantum interferences whose beating frequency, $\nu_b \approx 2.5 \times 10^{12}$ s^{-1}, is in reasonable agreement with QENS measurements [5]. Above T_c, quantum interferences for (11) are cancelled by symmetry. This is at odds with the expectation that fluctuations should increase at elevated temperatures. However, this fluctuation-free state cannot be 'observed' because QENS probes either $|P_u\rangle$ or $|P_d\rangle$ states.

Above T_c, diffuse scattering along (a^*), very slow dynamics, and enhanced diffraction suggest dynamical interconversion between superposed $|P_u\rangle$ and $|P_d\rangle$ states, on the one hand, and their analogues $|P2_1/a\rangle_u$ and $|P2_1/a\rangle_d$ states, on the other. This may occur through very small displacements of heavy atoms along (b) (figure 1). Upon cooling, symmetry breaking at T_c should lead to either $|P2_1/a\rangle_u$ or $|P2_1/a\rangle_d$ states, with equal probabilities. However, these structures are related through a translation vector $(a/2, b/2, 0)$. They are indistinguishable and the symmetry breaking leads to a unique $P2_1/a$ structure.

It is often argued that a complex open system undergoing continuous interactions with the environment should be in a significantly mixed state that cannot be represented by a state vector [51–53]. The present work leads to conclusions at variance with this view: the crystal of $KHCO_3$ at thermal equilibrium with the surrounding atmosphere can be represented by a state vector. The gaseous environment can

be treated as a distribution of plane waves that cannot destroy the entanglement intrinsic to the lattice periodicity. Only the spin symmetry can be transitory destroyed. However, this reversible disentanglement does not increase with time and it is insignificant because the density of states of the surroundings is smaller than that of the crystal by many orders of magnitude.

7. Conclusion

We confirm with single-crystal neutron diffraction the $C2/m$ structure composed of split C_i dimers proposed by Kashida and Yamamoto [9], but proton positions are at variance with those based on x-ray diffraction. The structure of the sublattice of protons is practically temperature independent, apart from site occupancies. The enhanced diffraction pattern measured at 340 K is basically identical to that arising from macroscopic quantum correlations below T_c [3, 4].

The theoretical framework for quantum correlations is based on fundamental principles of quantum mechanics. The fermionic nature of protons, unveiled by the adiabatic separation, leads to spin symmetry and super-rigidity. The spin symmetry is probed by neutrons diffracted at **Q**-values corresponding to nodes of the reciprocal lattice of protons. The coherent scattering cross-section is increased by a factor of ≈ 45, compared to that for uncorrelated protons, and super-rigidity cancels the shortfall of intensity by the Debye–Waller factor.

Above T_c, statistical disorder, or stochastic proton jumps, or clusters, or domains, or uncorrelated dynamics of individual dimers, or whatever phenomena which could destroy the translational invariance of the crystal, are excluded. The phase transition occurs from one ordered $P2_1/a$ structure to another ordered $C2/m$ structure. Both phases can be treated as pure states represented by state vectors. Raman spectroscopy and QENS show that eigenstates for protons are identical in the two structural phases. This suggests that the state vector $|C2/m\rangle$ is a superpositions of state vectors $|P_u\rangle$ and $|P_d\rangle$ for $P2_1/a$-like structures. This leads to the rather paradoxical conclusion that quantum interferences arising from superposition of proton states are cancelled by symmetry, as long as these states are not 'observed'.

This work emphasizes that atoms in the crystal field of $KHCO_3$ are not individual particles possessing properties on their own right. They merge into macroscopic states and exhibit all features of quantum mechanics: nonlocality, entanglement, spin symmetry, superposition and interferences. There is every reason to suppose that similar quantum effects should occur in many hydrogen bonded crystals undergoing structural phase transitions.

Acknowledgment

References

[1] Skinner J L and Trommsdorff H P 1988 Proton transfer in benzoic acid crystals: a chemical spin-boson problem. Theoretical analysis of nuclear magnetic resonance, neutron scattering, and optical experiments *J. Chem. Phys.* **89** 897–907

[2] Ikeda S and Fillaux F 1999 Incoherent-elastic-neutron scattering study of the vibrational dynamics and spin-related symmetry of protons in the $KHCO_3$ crystal *Phys. Rev.* B **59** 4134–45

[3] Fillaux F, Cousson A and Keen D 2003 Observation of the dynamical structure arising from spatially extended quantum entanglement and long-lived quantum coherence in the $KHCO_3$ crystal *Phys. Rev.* B **67** 054301
Fillaux F, Cousson A and Keen D 2003 Observation of the dynamical structure arising from spatially extended quantum entanglement and long-lived quantum coherence in the $KHCO_3$ crystal *Phys. Rev.* B **67** 189901 (erratum)

[4] Fillaux F, Cousson A and Gutmann M J 2006 Macroscopic quantum entanglement and super-rigidity of protons in the $KHCO_3$ crystal from 30 to 300K *J. Phys.: Condens. Matter* **18** 3229–49

[5] Fillaux F 2007 Proton transfer in the $KHCO_3$ and benzoic acid crystals: a quantum view *J. Mol. Struct.* **844/845** 308–18

[6] Eckold G, Grimm H and Stein-Arsic M 1992 Proton disorder and phase transition in $KHCO_3$ *Physica* B **180/181** 336–8

[7] Leggett A J 2002 Testing the limits of quantum mechanics: motivation, state of play, prospects *J. Phys.: Condens. Matter* **14** R415–51

[8] Haussühl S 1986 Anomalous elastic behaviour of monoclinic potassium hydrogen carbonate, $KHCO_3$, in the vicinity of the phase transition at 318 K *Solid State Commun.* **57** 643–7

[9] Kashida S and Yamamoto K 1990 Structural transition in $KHCO_3$ *J. Solid State Chem.* **86** 180–7

[10] Takasaka S, Tsujimi Y and Yagi T 1997 Acoustic anomaly in the antiferrodistortive phase transition of $KHCO_3$ studied by Brillouin scattering *Phys. Rev.* B **56** 10715–8

[11] Machida M, Yamaguchi Y, Sugimaya M, Iwata Y, Koyano N and Fukui S 1995 Neutron structural investigation of the isotope effect of $KHCO_3$ *Physica* B **213/214** 393–5

[12] Kanao R, Nohdo S-I, Horiuchi N, Kashida S, Kakurai K and Yamada Y 1996 Deuteron self-trapped state and the strain-mediated structural phase transition in $KDCO_3$ *J. Phys. Soc. Japan* **64** 2286–9

[13] Kanao R, Nohdo S-I, Horiuchi N, Kashida S, Kakurai K and Yamada Y 1996 Neutron scattering study on the structural phase transition in $KDCO_3$ *J. Phys. Soc. Japan* **65** 1710–7

[14] Kakurai K, Sakaguchi T, Nishi M, Zeyen C M E, Kashida S and Yamada Y 1996 Dynamics of the strain-mediated phase transition in $KDCO_3$: a thermal neutron spin-echo study *Phys. Rev.* B **53** R5974–7

[15] Yamada Y and Kanao R 1996 A note on the dynamical critical phenomena at the structural phase transition in $KDCO_3$ *J. Phys. Soc. Japan* **65** 1718–21

[16] Lim A R and Jeong S-Y 2001 Phase transition studied by nuclear spin–lattice relaxation in a $KHCO_3$ single crystal *Phys. Status Solidi* b **226** 413–8

[17] Lim A R and Jeong S-Y 2006 NMR study of the order–disorder phase transitions of $KHCO_3$ $KDCO_3$ single crystals *J. Solid State Chem.* **179** 1009–15

[18] Thomas J O, Tellegren R and Olovsson I 1974 Hydrogen-bond studies. LXXXIV. An x-ray diffraction study of the structures of $KHCO_3$ and $KDCO_3$ at 298, 219 and 95 K *Acta Crystallogr.* B **30** 1155–66

[19] Thomas J O, Tellegren R and Olovsson I 1974 Hydrogen bond studies. XCII. Disorder in $(HCO_3)_2^{2-}$ and $(DCO_3)_2^{2-}$ dimers: a neutron diffraction study of $KHCO_3$ and $KDCO_3$ *Acta Crystallogr.* B **30** 2540–9

[20] http://www-llb.cea.fr

[21] Watkin D J, Prout C K, Carruthers J R, Betteridge P W and Cooper R I 1996 Crystals issue 11 *Technical report Chemical Crystallography Laboratory (University of Oxford, England)*

[22] http://www.xtl.ox.ac.uk/crystals.html

[23] http://www.isis.rl.ac.uk/crystallography

[24] Keen D A, Gutmann M J and Wilson C C 2006 SXD—the single-crystal diffractometer at the Isis spallation neutron source *J. Appl. Crystallogr.* **39** 714–22

[25] Wilson C C 2002 Single crystal neutron diffraction from molecular materials *Series on Neutron Techniques and Applications* vol 2 (Singapore: World Scientific) p 912805

[26] Nield V M and Keen D A 2001 Diffuse neutron scattering from crystalline materials *Oxford Series on Neutron Scattering in Condensed Matter* vol 14 (Oxford: Clarendon)

[27] Novak A 1974 Hydrogen bonding in solids. Correlation of spectroscopic and crystallographic data *Struct. Bonding (Berlin)* **18** 177–216

[28] Schuster P, Zundel G and Sandorfy C 1976 The hydrogen bond *Recent Developments in Theory and Experiments* vol I, II and III (Amsterdam: North-Holland)

[29] Benderskii V A, Vetoshkin E V, Irgibaeva I S and Trommsdorff H P 2000 Tunneling splittings in vibrational spectra of non-rigid molecules: IX. malonaldehyde and its isotopomers as a test case for fully coupled multidimensional tunneling dynamics *Chem. Phys.* **262** 393–422

[30] Benderskii V A, Vetoshkin E V and Trommdorff H P 2001 Tunneling splittings in vibrational spectra of non-rigid molecules. X. Reaction path Hamiltonian as zero-order approximation *Chem. Phys.* **271** 165–182

[31] Giese K, Petrović M, Naundorf H and Kühn O 2006 Multidimensional quantum dynamics and infrared spectroscopy of hydrogen bonds *Phys. Rep.* **430** 211–76

[32] Smedarchina Z, Fernandez-Ramos A and Siebrand W 2005 Tunneling dynamics of double proton transfer in formic acid and benzoic acid dimers *J. Chem. Phys.* **122** 134309

[33] Tautermann C S, Voegele A F and Liedl K R 2004 The ground-state tunneling splitting of various carboxylic acid dimers *J. Chem. Phys.* **120** 631–7

[34] Benz S, Haeberlen U and Tegenfeldt J 1986 Jump motion of deuterons along hydrogen bonds in $KDCO_3$ a deuteron relaxation study *J. Magn. Reson.* **66** 125–34

[35] Fillaux F, Romain F, Limage M-H and Leygue N 2006 Extended tunnelling states in the benzoic acid crystal: infrared and raman spectra of the OH and OD stretching modes *Phys. Chem. Chem. Phys.* **8** 4327–36

[36] Maréchal Y and Witkowski A 1968 Infrared spectra of H-bonded systems *J. Chem. Phys.* **48** 3697–705

[37] Witkowski A 1967 Infrared spectra of the hydrogen-bonded carboxylic acids *J. Chem. Phys.* **47** 3645–8

[38] Fillaux F, Tomkinson J and Penfold J 1988 Proton dynamics in the hydrogen bond. The inelastic neutron scattering spectrum of potassium hydrogen carbonate at 5 K *Chem. Phys.* **124** 425–37

[39] Ikeda S, Kashida S, Sugimoto H, Yamada Y, Bennington S M and Fillaux F 2002 Inelastic neutron scattering study of the localized dynamics of protons in $KHCO_3$ single crystals *Phys. Rev.* B **66** 184302

[40] Kashida S, Ikeda S and Nakai Y 1994 Inelastic neutron scattering study of $KHCO_3$ *J. Phys. Soc. Japan* **63** 4643–7

[41] Cowley R A 2003 Quantum entanglement and neutron scattering experiments *J. Phys.: Condens. Matter* **15** 4143–52

[42] Keen D A and Lovesey S W 2003 Quantum correlation between protons in potassium bicarbonate *J. Phys.: Condens. Matter* **15** 4937–46

[43] Sugimoto H, Okumura A and Yuuki H 2006 Effects of entanglement on elastic and inelastic scattering functions for neutron scattering from a pair of nuclei in solids *Phys. Rev.* B **73** 014305

[44] Fillaux F and Cousson A 2004 Comment on quantum correlations between protons in potassium bicarbonate *J. Phys.: Condens. Matter* **16** 1007–10

[45] Leggett A J and Garg A 1985 Quantum mechanics versus macroscopic realism: is the flux there when nobody looks? *Phys. Rev. Lett.* **54** 857–860

[46] Lovesey S W 1984 *Nuclear Scattering, Theory of Neutron Scattered from Condensed Matter* vol I (Oxford: Clarendon)

[47] Odin C 2004 ^{13}C and ^{39}K high-resolution solid-state NMR study of the nonferroic phase transition of potassium hydrogen carbonate. Complementarity between NMR and incoherent neutron scattering *J. Phys. Chem.* B **108** 7402–11

[48] Fillaux F 1983 Calculation of infrared and Raman band profiles of strong hydrogen bonds. OH stretching band and proton dynamics in crystalline potassium hydrogen carbonate *Chem. Phys.* **74** 405–12

[49] Cohen-Tannoudji C, Diu B and Laloë F 1977 *Mécanique Quantique* (Paris: Hermann)

[50] Leggett A J 2005 The quantum measurement problem *Science* **307** 871–2

[51] Vedral V 2004 High-temperature macroscopic entanglement *New J. Phys.* **6** 102

[52] Jeong H and Ralph T C 2006 Transfer of nonclassical properties from a microscopic superposition to macroscopic thermal states in the high temperature limit *Phys. Rev. Lett.* **97** 100401

[53] Jeong H and Ralph T C 2007 Quantum superposition and entanglement of thermal states at high temperatures and their applications to quantum-information processing *Phys. Rev.* A **76** 042103